

# Excitation and visibility of slow modes in rotating B-type stars

W. A. Dziembowski<sup>1,2\*</sup>, J. Daszyńska-Daszkiewicz<sup>3</sup> and A. A. Pamyatnykh<sup>2,4</sup>

<sup>1</sup>Warsaw University Observatory, Al. Ujazdowskie 4, 00-478 Warsaw, Poland

<sup>2</sup>Copernicus Astronomical Center, Bartycka 18, 00-716 Warsaw, Poland

<sup>3</sup>Instytut Astronomiczny, Uniwersytet Wrocławski, ul. Kopernika 11, 51-622 Wrocław, Poland

<sup>4</sup>Institute of Astronomy, Russian Academy of Sciences, Pyatnitskaya Str. 48, 109017 Moscow, Russia

Accepted 2006 October 2; Received 2006 September 29; in original form 2006 July 7

## ABSTRACT

We use the traditional approximation to describe oscillations with frequencies comparable to the angular rotation rate. Validity of this approximation in application to main-sequence B stars is discussed. Numerical results regarding mode stability and visibility are presented for a model of the Be star HD 163868. For this object, Walker et al. (2005) detected a record number of mode frequencies using data from the small space telescope *MOST*. Our interpretation of these data differs from that of Walker et al. In particular, we interpret peaks in the lowest frequency range as retrograde g modes. We find instability in a large number of modes that remain undetectable because of unfavourable aspect and/or effect of cancellation. There is no clear preference to excitation of prograde modes.

**Key words:** stars: instabilities - stars: early-type - stars: emission-line, Be - stars: oscillation - stars: rotation.

## 1 INTRODUCTION

Results of linear stability calculations suggest that excitation of high-order g modes in main-sequence B-type stars must be a common phenomenon. The instability is typically robust. There is a significant excess of driving over damping and many modes are simultaneously unstable in individual stellar models. With the standard Population I composition, the instability is found in models of nearly all B-type stars. Yet, the observed pulsation associated with the slow modes is unspectacular. Individual modes never attain high amplitudes. Only in a small fraction of B stars do we have a firm evidence for the presence of oscillations and typically only few modes are seen. One possible reason why, despite strong instability, we never see high amplitude pulsation of this type is a collective saturation by a large number of modes which are difficult to detect. Recent report by Walker et al. (2005) on the detection of about sixty periods in the data on HD 163868 obtained from *MOST* may support this idea.

The fact that HD 163868 is a rapidly rotating Be type object makes the detection of many oscillation modes particularly interesting. The cause of activity observed in stars of this type is still not understood. Seismic constraints derived from mode frequencies on the internal structure would be of great value in this context. Furthermore, it is possible that

oscillations play an active role in these objects by inducing angular momentum transport, as first suggested by Osaki (1986) and Penrod (1986) and more recently, in the context of opacity-driven modes, by Lee (2006). Let us add that an asymmetry in excitation of prograde and retrograde modes may induce a net helicity of motion and thus an action of magnetic dynamo.

To extract seismic information, as well as to assess possible active role of oscillation, we have to identify modes excited in the star. The task of individual mode identification in an object like HD 163868 is formidable and will be attempted in this work. Like Walker et al. (2005), we will only try to determine angular degrees and azimuthal orders of the three groups of modes which are centered on periods of 8 days, and 14 and 7 hours. These authors, however, have not found unstable modes that could explain the longest period group.

We will argue that the observed modes represent only a small subset of the excited modes. Other modes having similar rms amplitudes may be not detectable because of cancellation and/or unfavourable aspect. Our analysis of stability and visibility is based on linear non-adiabatic calculations with the effects of rotation treated in the traditional approximation. The same approximations were adopted by Townsend (2005a,b) in his extensive survey of stability of slow modes in models of rotating main-sequence B-stars. The slow modes include high-order g modes with frequen-

\* E-mail: wd@astrouw.edu.pl

cies comparable to the angular rate of rotation and certain  $r$  modes (called mixed gravity-Rossby modes), which at sufficiently high rotation rate become propagatory in the radiative envelopes. Both types are candidates for identification of modes excited in HD 163868.

Our identification differs from that of Walker et al. (2005). One may suspect that the difference should be blamed to our use of the traditional approximation, which they avoid. However, as we explain in the next section, the approximation should be valid in the application to, at least, certain modes in HD 163868.

In Section 3, we present results on stability of slow modes in a model of HD 163868 which is very similar to the model used by Walker et al. (2005). We review properties of unstable modes in this and similar models and compare our results with those of our predecessors. In Section 4 we quantify the dependence of observable amplitude on the mode geometry and the aspect angle for the most unstable low-degree modes. Comparison with observations is presented in Section 5.

## 2 ON THE TRADITIONAL APPROXIMATION

There is a number of recent papers where *the traditional approximation* is used to describe properties of low frequency modes in rotating stars (e.g. Bildstein, Ushomirsky & Cutler 1996; Lee & Saio 1997; Townsend 2003a; Savonije 2005; Townsend 2005a,b). Readers are referred, in particular, to Townsend (2003a) for details of derivation of simplified equations for adiabatic oscillations known as *Laplace's Tidal Equations*, which employ the traditional approximation. The last three papers extend the approximation to the case of non-adiabatic oscillation. Here, we focus on the validity of approximation and its extension to the case of non-uniform rotation and we will quote only the most essential equations.

The generally adopted, initial simplifications of the linearized Euler equations,

$$\left(\frac{d\mathbf{v}}{dt}\right)' + \frac{1}{\varrho} \nabla p' - \frac{\varrho'}{\varrho^2} \nabla p + \nabla \Phi' = 0, \quad (1)$$

where all notation is standard, are (i) slow and (ii) uniform rotation, (iii) oscillation frequency,  $\omega$ , of the same order as the angular velocity of rotation,  $\Omega$ , (iv) neglect of  $\Phi'$  (the Cowling approximation), (v) adiabaticity of perturbations. Here we adopt (i) and (iii), that is, we assume

$$\frac{\omega^2 r}{g} \sim \frac{\Omega^2 r}{g} \equiv \epsilon \ll 1, \quad (2)$$

but not (ii) as we allow the  $r$  dependence in  $\Omega$ . Indeed, the traditional approximation applies to this more general case in the essentially unchanged form. We begin assuming (v) but later we will consider non-adiabatic effects, which are in fact of main interest for us in this paper.

Inequality (2) implies that the effects of centrifugal distortion may be neglected which together with (iv) reduces Eq. (1) to

$$\left(\frac{d\mathbf{v}}{dt}\right)' + \frac{1}{\varrho} \nabla p' + \frac{\varrho'}{\varrho} g \mathbf{e}_r = 0. \quad (3)$$

Since we allow non-uniform rotation, the constant eigenfrequency,  $\omega_{\text{obs}}$ , must be calculated in the inertial system, while

$\omega$  - the frequency calculated in the local corotating system - may vary with  $r$ . The acceleration in the inertial system expressed in terms of the displacement vector,

$$\boldsymbol{\xi} \equiv r \boldsymbol{\zeta}(r, \vartheta) \exp[i(m\varphi - \omega_{\text{obs}}t)], \quad (4)$$

is given by

$$\left(\frac{d\mathbf{v}}{dt}\right)' = -\omega^2 \boldsymbol{\xi} - 2i\Omega \boldsymbol{\omega} \mathbf{e}_z \times \boldsymbol{\xi} + (\mathbf{e}_r \sin \vartheta + \mathbf{e}_\vartheta \cos \vartheta) \frac{d\Omega^2}{dr} r \sin \vartheta \boldsymbol{\xi}_r, \quad (5)$$

where  $\omega(r) = \omega_{\text{obs}} - m\Omega(r)$ . Note that with the adopted form of the time dependence, the modes of azimuthal order  $m > 0$  are *prograde* and those with  $m < 0$  are *retrograde*. This is opposite to what has been adopted in the cited papers employing traditional approximation but it is in agreement with the *Çeşme Resolution* (see Appendix to Christensen-Dalsgaard & Dziembowski 2000).

Using the adiabaticity condition

$$\frac{\varrho'}{\varrho} = \frac{1}{\Gamma_1} \frac{p'}{p} + A \frac{\xi_r}{r}, \quad (6)$$

where we denoted

$$A = -\frac{d \ln \varrho}{d \ln r} - V_g \quad \text{and} \quad V_g = \frac{g r}{p \Gamma_1},$$

and introducing one additional eigenfunction,  $\zeta_p(r, \vartheta)$ , through the following identity

$$p' = g r \varrho \zeta_p(r, \vartheta) \exp[i(m\varphi - \omega_{\text{obs}}t)], \quad (7)$$

we get from Eq. (3)

$$\left(N^2 - \omega^2 + \frac{d\Omega^2}{dr} r \sin^2 \vartheta\right) \zeta_r + 2i\Omega \omega \sin \vartheta \zeta_\varphi + \frac{g}{r} \left(r \frac{\partial}{\partial r} + U - A - 1\right) \zeta_p = 0, \quad (8)$$

$$\frac{d\Omega^2}{dr} r \sin \vartheta \cos \vartheta \zeta_r - \omega^2 \zeta_\vartheta + 2i\Omega \omega \cos \vartheta \zeta_\varphi + \frac{g}{r} \frac{\partial \zeta_p}{\partial \vartheta} = 0, \quad (9)$$

and

$$2\Omega \omega \sin \vartheta \zeta_r + 2\Omega \omega \cos \vartheta \zeta_\vartheta - i\omega^2 \zeta_\varphi - \frac{mg}{r \sin \vartheta} \zeta_p = 0. \quad (10)$$

In Eq. (8) we use standard notation  $N$  for the Brunt-Väisälä frequency and  $U$  for the logarithmic derivative of the fractional mass. The continuity equation combined with Eq. (6) yields

$$\left(r \frac{\partial}{\partial r} + 3 - V_g\right) \zeta_r + \left(\frac{\partial}{\partial \vartheta} + \cot \vartheta\right) \zeta_\vartheta + \frac{im}{\sin \vartheta} \zeta_\varphi + V_g \zeta_p = 0, \quad (11)$$

which closes the system of equations for the eigenvalues  $\omega_{\text{obs}}$  and the associated eigenfunctions  $\zeta_r$ ,  $\zeta_\vartheta$ ,  $\zeta_\varphi$ , and  $\zeta_p$ .

In the traditional approximation all terms arising from the Coriolis force, except those in Eqs. (9) and (10) which contain horizontal components of  $\boldsymbol{\zeta}$ , are dropped out. A simple justification, based on the local wave approximation, was given by Lee and Saio (1997). The approximation is valid if

$$N = \sqrt{\frac{gA}{r}} \gg \Omega. \quad (12)$$

Earlier, the same condition was obtained by Dziembowski & Kosovichev (1987), who did not rely on the wave approximation and did not assume uniform rotation. Conditions (2) and (12) justify the neglect of those Coriolis terms

and the term containing the derivative of  $\Omega$ , both in the outer evanescent zone (assuming that it is radiative) as well as in the g-wave propagation zone. In both zones, we have  $|\zeta_\vartheta| \sim |\zeta_\varphi| \gg \max(|\zeta_r|, |\zeta_p|)$ , which justifies simplification of Eqs. (9) and (10). The relative scaling of  $\zeta_r$  and  $\zeta_p$  is different in the evanescent and g-wave zone. In the former, where  $V_g$  and  $A$  are large,  $|\zeta_r| \sim |\zeta_p| \sim \epsilon \zeta_\vartheta \sim \epsilon \zeta_\varphi$  and the simplification in Eq. (8) follows from  $A \gg 1$ . In the propagation zone, where the mode amplitude varies rapidly, we have

$$\left| r \frac{\partial \zeta_p}{\partial r} \right| \sim \sqrt{\frac{N}{\Omega}} |\zeta_p| \sim \frac{A}{\epsilon} |\zeta_r| \gg |\zeta_\varphi| \gg |\zeta_r|,$$

which justifies the neglect of all terms containing  $\Omega$ . Note that the  $\omega^2$  term in the coefficient at  $\zeta_r$  could have been ignored too but traditionally this is not done.

With the traditional approximation, the  $r$  and  $\vartheta$  dependence in the eigenfunctions may be separated. The latter dependence is given by the Hough functions. Following Townsend (2003a), we substitute in Eqs. (8-11)

$$\zeta_r = y_1(r)\Theta(\vartheta), \quad \zeta_p = y_2(r)\Theta(\vartheta) \quad (13)$$

$$\sin \vartheta \zeta_\vartheta = z(r)\hat{\Theta}(\vartheta), \quad \text{and} \quad i \sin \vartheta \zeta_\varphi = z(r)\tilde{\Theta}(\vartheta) \quad (14)$$

to obtain ordinary differential equations for  $y_1$  and  $y_2$ ,

$$r \frac{dy_1}{dr} = (V_g - 3)y_1 + \left( \frac{\lambda g r}{\omega^2} - V_g \right) y_2, \quad (15)$$

and

$$r \frac{dy_2}{dr} = \left( \frac{r\omega^2}{g} - A \right) y_1 + (A + 1 - U)y_2, \quad (16)$$

where, for a uniform rotation,  $\lambda$  is the separation parameter. The radial dependence for the horizontal components of  $\xi$  is given by

$$z = \frac{g}{r\omega^2} y_2. \quad (17)$$

Eqs. (15) and (16) look just like in the case of no rotation, except that now we have  $\omega = \omega_{\text{obs}} - m\Omega$  and in the place of  $\ell(\ell + 1)$  the separation parameter  $\lambda$ , which is determined as an eigenvalue in the equations for the Hough functions. We write these equations in the form

$$\tilde{\Theta} = -m\Theta + s\mu\hat{\Theta} \quad (18)$$

$$(1 - \mu^2) \frac{d\Theta}{d\mu} = -ms\mu\Theta + (s^2\mu^2 - 1)\hat{\Theta} \quad (19)$$

$$(1 - \mu^2) \frac{d\hat{\Theta}}{d\mu} = [\lambda(1 - \mu^2) - m^2]\Theta + ms\mu\hat{\Theta}, \quad (20)$$

where  $\mu \equiv \cos \vartheta$  and  $s \equiv 2\Omega/\omega$  is called *the spin parameter*. Eqs. (19-20) differ from Townsend's Eqs. (21-22) only in the sign of  $s$ , which he denoted  $\nu$ , in consequence of different sign convention for the time dependence. The equations together with boundary conditions at  $\mu = 0$  (symmetry) and  $\mu = 1$  (regularity) define the eigenvalue problem on  $\lambda$ . The dependence of  $\lambda$  on  $s$  and related properties of the Hough functions have been discussed in great detail by, for example, Bildstein et al. (1996), Lee & Saio (1997), and by Townsend (2003a).

Of our interest here are only modes which are propagating in radiative zones, where  $A > 0$ , that is, corresponding

to  $\lambda > 0$ . These are the g modes for which  $\lambda \rightarrow \ell(\ell + 1)$  at  $s \rightarrow 0$ , as well as the mixed gravity-Rossby modes, for which  $\lambda$  changes sign from minus to plus at  $s = |m| + 1$  (for brevity, in this paper, we shall call them r modes). It was shown, independently by Townsend (2005b) and Savonije (2005) and confirmed by Lee (2006), who did not use the traditional approximation, that such modes may be driven in B-type and early A-type stars. Let us note that if  $\Omega$  is a function of  $r$ , then such modes may be trapped in the region of rapid rotation where  $\lambda > 0$  while it is  $< 0$  in the rest of the star interior.

In the case of massive main-sequence stars, the traditional approximation cannot be used in their convective cores. However, low frequency waves do not propagate there and thus the core surface may be treated as a boundary. Except for zero-age main-sequence stars there is a nearly discontinuous transition at the core edge,  $r = r_c$ , from  $N \gg \Omega$  to  $N \approx 0$ . In the core,  $\zeta_p$  and other eigenfunctions are slowly varying with distance from the center. Thus, with  $N \approx 0$ , Eq. (8) implies

$$|\zeta_p| \sim \epsilon |\zeta_r| \quad \text{for } r \leq r_c. \quad (21)$$

On the other hand, in the propagation zone, we have  $k_r \zeta_p \approx N^2 \zeta_r / g$ , where the local radial wave number is given by  $k_r = k_H N / \omega$  and  $k_H = \sqrt{\lambda} / r$  is the horizontal wave number. Hence,

$$|\zeta_p| \sim \sqrt{\epsilon \frac{A}{\lambda}} \quad \text{for } r \geq r_c. \quad (22)$$

Since there is no jump of density at  $r = r_c$ , the continuity of  $\delta p$  and  $\xi_r$  imply the continuity of  $\zeta_p$ . Thus, from Eqs. (21) and (22), we get the boundary condition consistent with the traditional approximation to be imposed on solutions of Eqs. (15) and (16),

$$\frac{y_2(r_c)}{y_1(r_c)} \sim \sqrt{\epsilon} \approx 0. \quad (23)$$

In stars of our interest, there are thin convective layers, connected with the HeII ionization and, if  $M \gtrsim 7M_\odot$ , with the Fe opacity bump. Because of their small vertical extent, such layers cannot affect significantly global mode geometry.

The two boundary conditions, which should be applied on solution of Eqs. (15-16), are

$$y_2 = 0 \text{ at } r = r_c \quad \text{and} \quad y_2 = y_1 \text{ at } r = R. \quad (24)$$

The same boundary conditions remain valid when non-adiabatic effects are taken into account.

Eqs. (15-20) remain valid in the case of shellular rotation but then, both  $\omega$  and  $\lambda$  must be regarded as functions of  $r$ . The derivation given by Dziembowski & Kosovichev (1987) employed expansion of the  $\theta$  dependence in a series of the associated Legendre functions. Assuming  $\Omega/N \sim \delta \ll 1$ , they decomposed the infinite system of differential equations in  $r$  into asymptotically independent second-order equations equivalent, in the limit  $\delta \rightarrow 0$ , to Eqs. (15-16). In their derivation there is an inconsequential omission of terms  $\sim \delta d \ln \Omega / d \ln r$  and an implicit assumption that the logarithmic derivative of  $\Omega$  is of the order of 1.

Townsend (2005a) and Savonije (2005) extended the traditional approximation to the case of non-adiabatic oscillations. Using the same equation as in the case of no rotation with only  $\lambda$  in place of  $\ell(\ell + 1)$  is incorrect in the expression

for the horizontal heat losses. However, these losses, which are proportional to  $k_H^2$ , make rather small contribution to the overall work integral. Another simplification is the use of  $\lambda$  with  $\omega$  calculated in the adiabatic approximation. This is well justified in our applications because the non-adiabatic change in  $\omega$  is very small.

Lee & Saio (1989) pointed out that even at  $\delta \ll 1$  coupling between modes of close frequencies, the same  $m$  and symmetry may have a significant effect. In a specific example of  $4M_\odot$  star sequence, Lee (2001) found that some modes, which are unstable if the traditional approximation is used, are found stable if the approximation is abandoned and the truncated expansion in Legendre functions is used for the eigenfunctions. However, many modes remained unstable and we expect that this applies also in the case of models considered in this paper. We will discuss this matter further in Section 3.

### 3 UNSTABLE MODES

With the traditional approximation, stability properties of slow modes are determined by two parameters:  $\lambda$  and  $\omega$ . In this section, we assume uniform rotation, hence  $\omega$  is the mode eigenfrequency in the corotating system. The whole influence of rotation and the azimuthal order is absorbed in the  $\lambda(s)$  dependence. Thus, like in the case of no rotation, we deal with a two-dimensional instability range for a specified model. In the present case, the two parameters are  $\omega$  and  $\sqrt{\lambda}/\omega$ . The latter determines radial order of the mode,  $n$ , and the  $r$  dependence of the Lagrangian pressure perturbation,  $\delta p/p$ . For instability, the amplitude of the perturbation should be large and slowly varying in the layer of the iron opacity bump. The frequency,  $\omega$ , determines resulting perturbation of the radiative flux. Furthermore, a match is needed between the thermal time-scale of this layer,  $\tau_{\text{th}}$ , and the pulsation period,  $\Pi = 2\pi/\omega$ .

The instability ranges in terms of  $\ell$  and  $\omega$  for non-rotating main-sequence B-stars were discussed in detail by Dziembowski, Moskalik & Pamyatnykh (1993) and by Pamyatnykh (1999). A corresponding discussion for rotating stars was presented recently by Townsend (2005a). For a family of stellar models,  $\sqrt{\lambda}/\omega$  does not determine mode order but still, to a large extent, determines the shape of the pressure eigenfunction in the outer layers, which bring the main contribution to the work integral. Thus, the evolutionary radius increase results in longer periods of unstable modes. The associated decrease of the effective temperature, causing an increase of  $\tau_{\text{th}}$ , acts in the same direction. This is why the initial effect of evolution is an enhancement of instability. The tendency is reversed only near the end of the main-sequence evolution when dissipation in the g-wave propagation zone becomes significant. Too small values of  $\tau_{\text{th}}$  are the cause why the modes with low values of  $\lambda$  are stable in massive ( $M \gtrsim 4.5M_\odot$ ) hot objects.

In this paper we present numerical results for a single stellar model calculated with Warsaw-New Jersey stellar evolutionary code (see e.g. Pamyatnykh 1999) assuming no mixing beyond the convective core and including only mean effect of the centrifugal force. The same approximations were adopted by Walker et al. (2005). Our model is characterized by the following parameters:  $M = 6M_\odot$ ,  $X_0 = 0.7$ ,  $Z = 0.02$ ,

$X_c = 0.307$ ,  $\log T_{\text{eff}} = 4.226$ ,  $v_{\text{rot}} = 300$  km/s, which are very similar to those used by these authors.

Our non-adiabatic pulsation code uses the same approximation as adopted by Townsend (2005a) except that we apply the inner boundary condition  $y_2 = 0$  at the edge of convective core. The code is almost a trivial modification of our standard nonradial pulsation code in its version adopting the Cowling approximation, which is indeed very accurate for all considered modes. In the adiabatic part of the code values of  $\lambda$  are interpolated from the tables of  $\lambda(s)$  prepared with a separate code for all types of modes of our interest. The values were not changed in the non-adiabatic part. We focused the main attention on modes which may be driven by the opacity mechanism and are potentially detectable by photometry. Thus, the modes considered have  $\lambda$  greater than zero but not too large. For each  $|m| \leq 2$ , we included g modes with the lowest values  $\lambda$ . Sequences of modes of different radial order are denoted with  $(\ell, m)$ , where  $\ell(\ell+1) = \lambda(0)$ . We also included two sequences of lowest order retrograde r modes with  $\lambda > 0$  for  $s > |m| + 1$ . The mode instability is characterized by the normalized work integral

$$\eta = \frac{W}{\int_0^R \left| \frac{dW}{dr} \right| dr}, \quad (25)$$

where  $W$  is the usual work integral. The growth rate,  $\Im(\omega)$ , has the same sign but its value is affected mostly by mode inertia. The value of  $\eta$ , which varies between -1 and 1, is a better measure of robustness of the instability and a better predictor of the mode amplitude. Fig. 1 shows the values of  $\eta$  for all considered modes in their range of instability and close to it. Table 1 provides more information about most unstable modes (largest  $\eta$ ).

The instability range in the observed frequencies,  $\nu_{\text{obs}} = \omega_{\text{obs}}/2\pi$ , extends from nearly zero for retrograde  $\ell = 1$  g modes to 4 c/d for prograde  $\ell = 2$  modes. The former modes have frequencies in the vicinity of  $\nu_{\text{rot}} = \Omega/2\pi$ . The modes with frequencies  $\nu_{\text{star}} = \omega/2\pi < \nu_{\text{rot}}$  are seen as prograde modes. The range of frequencies in the corotating system is much narrower. We may see in Table 1 that the most unstable modes occur near  $\nu_{\text{star}} \approx 1.6$  c/d,  $\lambda \approx 30$  and  $n = 20$ . The prograde  $\ell = 1$  modes have  $\lambda < 2$  and, thus, at  $\sqrt{\lambda}/\omega$  values favourable for driving, too long periods. Such modes were found unstable in somewhat cooler models. A lower value of  $T_{\text{eff}}$  would also result in lower  $\nu_{\text{star}}$  of the unstable modes. The shift in  $\nu_{\text{obs}}$  is the same but, if  $m\nu_{\text{rot}} > \nu_{\text{star}}$ , of opposite sign. In the vicinity of our model a shift of 0.01 in  $T_{\text{eff}}$  leads to the 0.1 c/d frequency shift of most unstable modes. A change in the adopted value of  $v_{\text{rot}}$  would shift the instability ranges in  $\nu_{\text{obs}}$  for  $m \neq 0$  modes.

There are many more strongly unstable modes than shown in Fig. 1. The instability continues up to  $\lambda \approx 600$ . Modes with  $\eta > 0.2$  are found up to  $\lambda \approx 120$ , which corresponds to  $m = 11$  for sectorial prograde modes. Owing to higher  $\lambda$  values such modes are subject to much larger observable amplitude reduction. Visibility of modes is the subject of the next section. Here, we just want to point out that we should expect in any of multiperiodic B-type star many more excited modes than those detected. Such modes have properties similar to those listed in Table 1, except they would have much lower surface averaged amplitudes. Possible excitation of many unobservable modes must be kept in

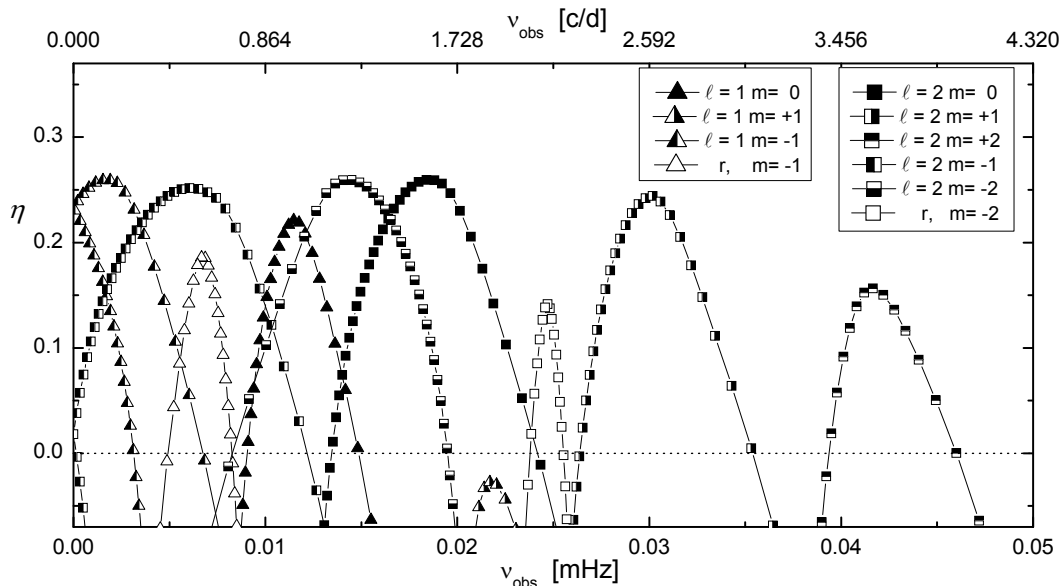


**Figure 1.** The instability parameter,  $\eta$  (see Eq.(25)) as function of frequency for slow modes of low azimuthal orders in the model of HD 163868. The frequencies are calculated in the inertial system. The frequency of rotation is  $\nu_{\text{rot}} \equiv \Omega/2\pi = 1.42$  c/d.

**Table 1.** Parameters of the most unstable modes with  $|m| \leq 2$  for the stellar model with  $M = 6.0M_{\odot}$ ,  $\log T_{\text{eff}} = 4.226$ ,  $\log L/L_{\odot} = 3.094$ , and a rotational velocity of 300 km/s, which corresponds to  $\nu_{\text{rot}} = 1.4165$  c/d. See Eq.(29) for the definition of  $f$ .

$\ell$	$m$	$n$	type	parity	$\nu_{\text{obs}}$ [c/d]	$\nu_{\text{star}}$ [c/d]	spin	$\lambda$	$\eta$	$f$
1	0	20	zonal, g	odd	0.9911	0.9911	2.86	8.76	0.221	(7.67, 12.96)
1	1	15	progr, g	even	1.8748	0.4582	6.18	1.09	-0.027	(9.46, 9.00)
1	-1	21	retro, g	even	0.1654	1.5819	1.79	24.69	0.259	(1.15, 8.93)
	-1	19	retro, r	odd	0.5772	0.8393	3.38	5.70	0.186	(8.94, 12.68)
2	0	20	zonal, g	even	1.5893	1.5893	1.78	27.29	0.259	(1.78, 9.70)
2	1	20	progr, g	odd	2.6081	1.1916	2.38	12.71	0.244	(4.65, 11.58)
2	2	18	progr, g	even	3.5997	0.7666	3.70	4.28	0.156	(8.69, 11.88)
2	-1	23	retro, g	odd	0.5228	1.9393	1.46	45.07	0.252	(-0.51, 6.60)
2	-2	22	retro, g	even	1.2515	1.5816	1.79	27.02	0.259	(1.85, 9.78)
	-2	19	retro, r	odd	2.1348	0.6983	4.06	3.94	0.142	(11.71, 12.93)

mind while considering the feedback of oscillations on stellar rotation. The results shown in Fig. 1 and in Table 1 might suggest that there is preference to retrograde mode excitation but it is not found in the full set of the unstable modes. For instance,  $\eta \geq 0.2$  was found in over 450 prograde modes, and in less than 370 retrograde modes. Certainly, there is no evident asymmetry in driving prograde and retrograde modes.

Our findings regarding mode instability differ from that presented by Walker et al. (2005). Unlike these authors, we do not find instability of the prograde  $\ell = 1$  modes. On the other hand, we find many retrograde  $\ell = 1$  modes, which may account for the longest periods measured in HD 163868, whereas no instability of such modes was found in that work. The general pattern of the difference is that we find instability in many more modes with higher  $\lambda$ . Perhaps the tra-

ditional approximation, which we rely on, is not applicable. The mode coupling, as described by Lee (2001), may stabilize only certain modes. Could it stabilize all retrograde  $\ell = 1$  modes and destabilize all prograde  $\ell = 1$  modes? We do not know the answers. Perhaps, there is a difference in internal structure between the models used by us and that used by Walker et al. (2005). We should also be aware that the Lee & Saio method, which is based on a truncated series expansion, used in that paper, may not be accurate.

Considering possible identification of modes detected in HD 163868, we should take into account visibility conditions for modes described by the Hough functions.

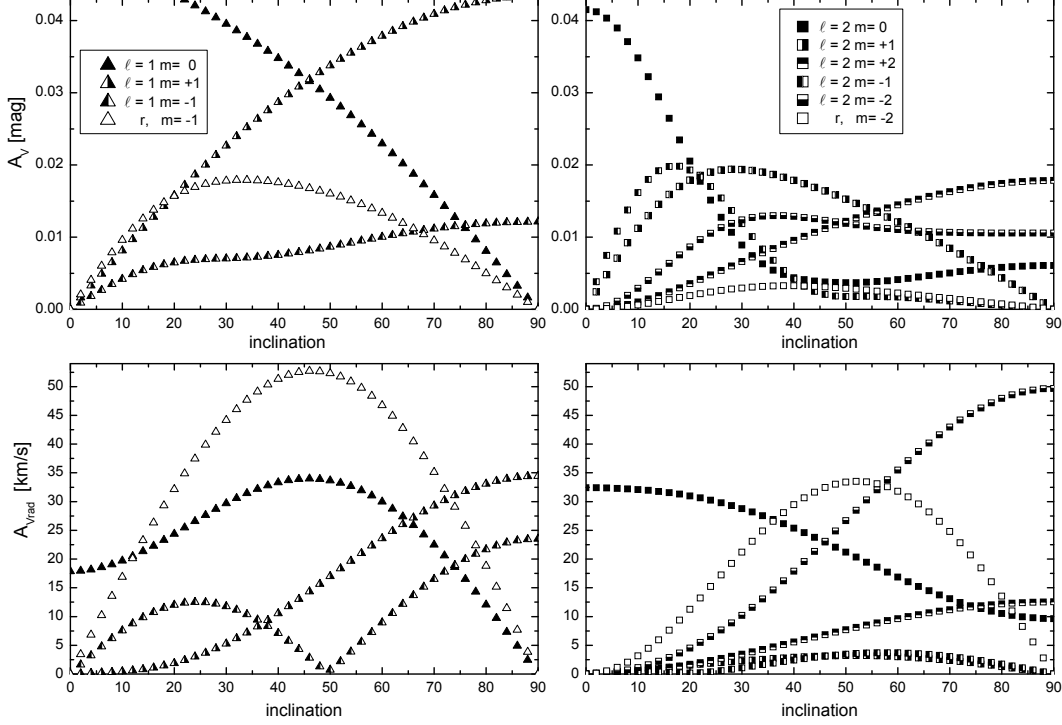


**Figure 2.** Light amplitudes in the Geneva  $V$  band (upper panels) and in radial velocity (lower panel) as functions of the inclination angle for modes listed in Table 1.

#### 4 VISIBILITY

Observed amplitude of a mode depends on its true amplitude, geometry and the aspect angle,  $i$ . Photometric amplitudes for modes described by single spherical harmonics were calculated in a number of papers. Results of corresponding calculations for modes described by the Hough functions were first published by Townsend (2003b), who relied on truncated expansion of  $\Theta$  in associated Legendre functions. In our calculations of the photometric and radial velocity amplitudes, we avoid such expansion and carry out two-dimensional integration over visible hemisphere. Details of our approach and a survey of the results will be published elsewhere (Daszyńska-Daszkiewicz et al., in preparation). Here we quote only the background formulae and present discussion of visibility of modes listed in Table 1 as a function of aspect.

Within the linear non-adiabatic theory, there is a freedom in normalization of eigenfunctions. Here we adopt the most common one, that is  $y_1(R) = 1$ , and

$$\int_0^1 \Theta^2 d\mu = 1.$$

Thus, we write

$$\xi_r(R) = \varepsilon R \Theta Z, \quad (26)$$

where  $Z = \exp[i(m\varphi - \omega t)]$ . The value of  $|\varepsilon|$  (not to be confused with  $\varepsilon$  in Section 2) determines true mode amplitude. Note that the surface displacement is given by  $\Re[\xi_r(R)]$  and its rms value is equal to  $|\varepsilon|/\sqrt{4\pi}$ . The surface boundary condition,  $y_2(R) = y_1(R)$ , combined with Eqs. (4) and (14) leads to the following expressions for the horizontal components

of the displacement

$$\xi_\theta = \varepsilon \frac{GM}{\omega^2 R^2} \frac{\hat{\Theta}}{\sin \vartheta} Z \quad (27)$$

and

$$\xi_\varphi = -i\varepsilon \frac{GM}{\omega^2 R^2} \frac{\tilde{\Theta}}{\sin \vartheta} Z. \quad (28)$$

These components are needed only for calculation of the pulsation velocity field.

For evaluation of the photometric amplitudes, we need a linear relation between the radial components of displacement and perturbed flux which we write in the form

$$\frac{\delta \mathcal{F}_{\text{bol}}}{\mathcal{F}_{\text{bol}}} \equiv 4 \frac{\delta T_{\text{eff}}}{T_{\text{eff}}} = \varepsilon f \Theta Z, \quad (29)$$

where  $f$  is a complex coefficient determined from linear non-adiabatic calculations. Its values for modes considered are given in the last column of Table 1. In order to calculate the flux in a specified band,  $x$ , we need also an expression for the perturbed surface gravity, which is

$$\frac{\delta g}{g} = -\varepsilon \left( \frac{r\omega^2}{g} + 2 \right) \Theta Z \approx 2\Theta Z,$$

and the perturbed surface element,

$$\frac{\delta d\mathbf{S}}{d\mathbf{S}} = \varepsilon \left( 2\Theta, -\frac{\partial \Theta}{\partial \theta}, -\frac{im\Theta}{\sin \theta} \right) Z,$$

where  $d\mathbf{S} = R^2 d\mu d\varphi$ . The tangential components arise from the change of the normal to the stellar surface. These components are needed also in the expression for the perturbed limb-darkening,  $\delta h_x$ . The perturbed flux is thus given by

$$\delta L_x = \int_S [(\delta \mathcal{F}_x h_x + \mathcal{F}_x \delta h_x) d\mathbf{S} e_r + \mathcal{F}_x h_x \delta d\mathbf{S}] \cdot \mathbf{n}_{\text{obs}}, \quad (30)$$

where  $x$  represents a photometric band,  $\mathbf{n}_{\text{obs}}$  is the unit vector toward observer, and the integration is done over the visible unperturbed hemisphere. The limb-darkening coefficient is normalized, so that

$$L_x = \int_S \mathcal{F}_x h_x \tilde{\mu} dS,$$

where  $\tilde{\mu} = \mathbf{n}_{\text{obs}} \cdot \mathbf{e}_r$ . Static atmosphere models are used to calculate wavelength-dependent flux,  $\mathcal{F}_x(T_{\text{eff}}, g)$ , and the limb-darkening coefficient,  $h_x(T_{\text{eff}}, g)$ .

The disc-averaged change of radial velocity is given by the expression

$$\langle v_{\text{rad}} \rangle = L_x^{-1} \int_S (\mathbf{v}_{\text{puls}} + \mathbf{v}_{\text{rot}}) \cdot \mathbf{n}_{\text{obs}} \mathcal{F}_x h_x \mathbf{n}_{\text{obs}} \cdot d\mathbf{S}, \quad (31)$$

where

$$\mathbf{v}_{\text{puls}} = \frac{d\xi}{dt} \quad \text{and} \quad \mathbf{v}_{\text{rot}} = R\Omega \sin \vartheta \mathbf{e}_\varphi$$

In the linear approximation, the contribution from the first term may be calculated with unperturbed  $h$ ,  $\mathcal{F}$ , and  $\mathbf{S}$ . The contribution from the second term arises solely from perturbation of these quantities. Thus, the radial velocity change is given by

$$\langle v_{\text{rad}} \rangle = \int_S \left\{ \left[ \mathbf{v}_{\text{puls}} + \left( \frac{\delta \mathcal{F}_x}{\mathcal{F}_x} + \frac{\delta h_x}{h_x} \right) \mathbf{v}_{\text{rot}} \right] \cdot \mathbf{n}_{\text{obs}} \tilde{\mu} + (\mathbf{v}_{\text{rot}} \cdot \mathbf{n}_{\text{obs}}) \frac{\delta d\mathbf{S}}{dS} \cdot \mathbf{n}_{\text{obs}} \right\} \mathcal{F}_x h_x dS. \quad (32)$$

We show in Fig. 2 the amplitudes of light and radial velocity as functions of the inclination angle for the modes listed in Table 1. These amplitudes are calculated with the arbitrary choice  $|\varepsilon| = 0.01$  and for the Geneva  $V$  band, which is similar to Johnson's  $V$ . The plotted quantities are

$$A_V = 1.086 \left| \frac{\delta L_x}{L_x} \right| \quad \text{and} \quad A_{\text{vrad}} = |\langle v_{\text{rad}} \rangle|.$$

In the dependence  $A_V(i)$ , we see certain patterns which are the same as for modes described by single spherical harmonics. Zonal modes are best seen from near polar direction, while symmetric (even) modes are best seen from near equatorial direction. There are, however, significant differences. In particular, an increase of  $\lambda$  does not lead to so large amplitude reduction as expected from the  $\ell(\ell+1) \rightarrow \lambda$  replacement. Compare, for instance, two sectorial  $\ell = 1$  modes. There is the factor 25 difference in  $\lambda$  between  $m = -1$  and  $m = +1$  modes and only the factor 4 in  $A_V$ , while the factor  $\sim 12$  would be expected in the non-rotating case, on the basis of the decline of the disc-averaging factor,  $b_\ell$ , with  $\ell$  (e.g. Dziembowski 1977). According to our calculations the  $m = +1$  mode is stable. Among unstable modes, the  $(\ell = 1, m = -1)$  is the second best visible, after  $(\ell = 2, m = +2)$ , from the near equatorial directions. Despite of near-equatorial trapping caused by rotation, the optimum inclination for detection of tesseral modes, such as  $(\ell = 2, m = \pm 1)$ , is shifted toward the pole because then cancellation of contributions from the two hemispheres, which have opposite signs, is reduced. Such a cancellation is responsible for rather low amplitudes of the r modes.

The behaviour of the radial velocity amplitudes, depicted in the lower panels of Fig. 2, shows rather different pattern. At intermediate inclinations of the rotation axis,

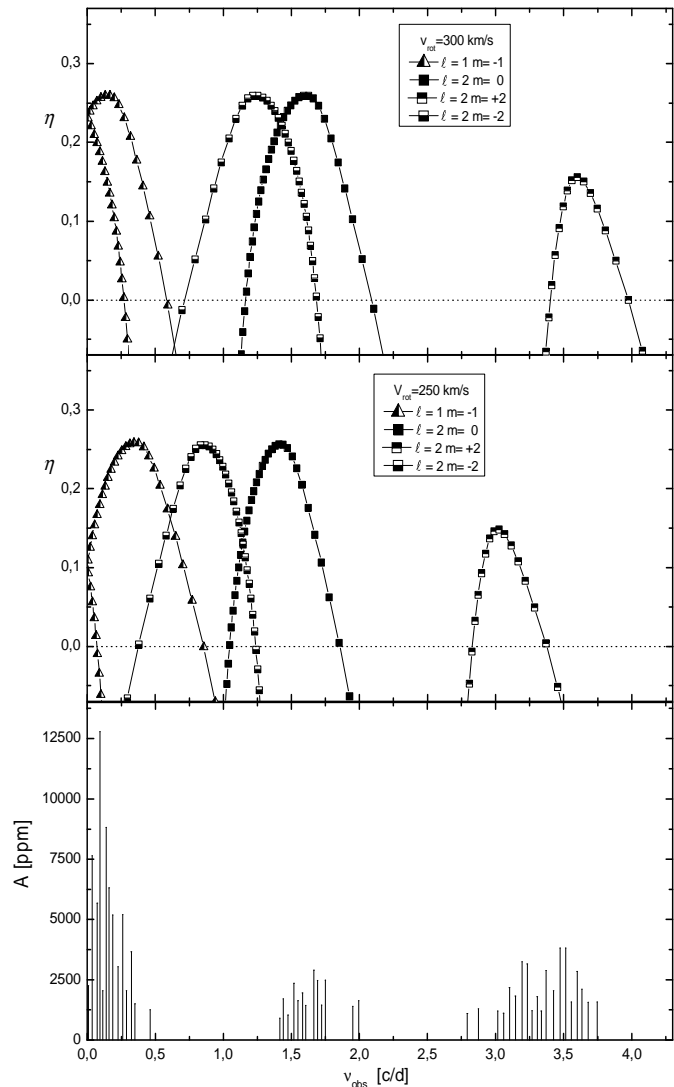


**Figure 3.** Growth rates for symmetric (even) modes, which are preferentially visible from the near equatorial directions (see Fig. 2), in models of HD 163868 calculated with two indicated equatorial velocities of rotation (the upper panels) and amplitudes the peaks detected in the *MOST* data.

the r modes turn out most easily detectable. At large inclinations (near equatorial observer) the modes  $|m| = \ell$  are best seen both in light and radial velocity variations. However, the ratio exhibits a strong mode dependence. Interpretation of the radial velocity amplitude pattern is complicated because the contribution from pulsation and rotation are of comparable size. Here we would like only to stress that the strong mode dependence of the amplitude ratios points to the good prospect for mode identification by combining spectroscopy and photometry data.

## 5 PEAKS IN THE HD 163868 OSCILLATION SPECTRUM

The measured value of  $v \sin i$  in HD 163868 is high. Therefore, we assume that the star is seen from a near equatorial

direction and, as possible candidates for identification, we consider only symmetric modes.

There are three groups of frequencies found by Walker et al. (2005) in the star. That with  $\nu_{\text{obs}} < 0.5$  c/d could only be interpreted in terms of the retrograde  $\ell = 1$  modes. Possible interpretations for the group with  $\nu_{\text{obs}}$  between 1.4 and 2 c/d are  $\ell = 2$  modes with  $m = -2$  and  $m = 0$ . For the group with  $\nu_{\text{obs}}$  between 2.8 and 3.75 the only interpretation is  $\ell = 2, m = +2$ . In this last case our mode identification is the same as that of Walker et al. (2005).

In Fig. 3 we see that our interpretation is also not fully satisfactory though, unlike our predecessors, we have no difficulty with interpretation of lowest frequency group, where the highest amplitudes are found. Just like theirs, our predicted range at the highest frequencies is somewhat narrow. The largest discrepancy between results of our calculation and observation is for the intermediate group. Certainly, the discrepancy may be reduced by adjusting  $v_{\text{rot}}$  and  $T_{\text{eff}}$ .

It is possible that the some of the peaks in the HD 163868 oscillation spectrum, in particular those in the low frequency range, are artefacts of the data processing. Interpretation of peaks in terms of specific modes should be tested with simultaneous multiband photometry and radial velocity data. We have seen in the previous section that the ratio of radial velocity to light amplitude is strongly mode dependent and it is exceptionally large for the retrograde  $\ell = 1$  modes, which may explain peaks in the low frequency range. The dominant peak in this range and in the whole oscillation spectrum has photometric amplitude of 0.013 mag in the *MOST* photometric system. Assuming that the amplitude in the *V* band is similar and using plots in Fig. 2, we find radial velocity amplitude of about 30 km/s, which should be easily measured in radial velocity data spanning sufficiently long time interval.

## 6 CONCLUSIONS

Data on oscillations in Be stars may be helpful in explaining activity of these stars. The application is twofold. Firstly, the data may be a source of seismic information on internal rotation. Secondly, the data may allow to assess the role of the feedback effect of oscillation in these stars. Both aims require identification of modes detected in the observed oscillation spectra. The clue to identification which may be provided by the theory is the determination of a set of modes that may be excited and detected.

Effects of rotation, which are important in Be star oscillations, must be taken into account. This is most easily done with the traditional approximation. Validity of this approximation in application to slow modes in Be stars, we discussed in Section 2. We applied our non-adiabatic version of this approximation to a model of HD 163868, the first Be star with the rich oscillation spectrum. The spectrum, determined from the *MOST* photometric satellite data, and its preliminary partial interpretation, has been recently published by Walker et al. (2005).

We showed that there is a large number of unstable modes in the model of this star, covering the whole frequency range of the peaks in the HD 163868 spectrum and beyond. The instability extends to modes of high horizontal degrees, corresponding to  $\ell \approx 24$  in the case of no rotation. We found

no significant difference in driving between prograde and retrograde modes.

Our calculations of the relative visibility of the unstable modes show that the three consecutive groups of the peaks may be explained by low-degree high-order g modes seen from the near equatorial direction. Specifically, the group with frequencies below 0.5 c/d may be explained by retrograde  $\ell = 1$  modes, the group around 1.7 c/d by retrograde sectorial and zonal  $\ell = 2$  modes the group around 3.5 c/d by prograde sectorial  $\ell = 2$  modes. Only the interpretation of the highest frequency group is the same as that proposed by Walker et al. They interpret the intermediate group in terms of  $\ell = 1$  prograde mode, which we find stable. In contrast, the modes that we associate with this group are found stable in their calculations. Also they found all retrograde  $\ell = 1$  modes to be stable and therefore did not find a satisfactory interpretation for the lowest frequency group, where peaks have the highest amplitudes. They proposed that some of the peaks in this group may be interpreted in terms of retrograde r modes, which are found unstable, both by them and us, but their interpretation leaves unexplained highest peaks and there is also a problem with the visibility of such modes from the nearly equatorial direction. A possible cause of the difference in interpretation of the same data is the use of very different approximations in the treatment of the difficult problem of slow oscillations in rotating stars.

## ACKNOWLEDGMENTS

We thank the referee, Rich Townsend, for his comments which have significantly helped us to improve the manuscript, and Hideyuki Saio for a conversation that also had an impact on the final version of this paper. This investigation has been supported by the Polish MNiI grant No. 1 P03D 021 28.

## REFERENCES

- Bildstein L., Ushomirsky G., Cutler, C., 1996, ApJ, 460, 827
- Christensen-Dalsgaard, J., Dziembowski, W. A., 2000, in Variable Stars as Essential Astrophysical Tools, ed. C. Ibanoglu (NATO ASI Ser. C, 544; Dordrecht: Kluwer), 1
- Dziembowski W. A., 1977, Acta Astr., 27, 203
- Dziembowski W. A., Kosovichev A., 1987, Acta Astr., 37, 313
- Dziembowski W. A., Moskalik P., Pamyatnykh A. A., 1993, MNRAS, 265, 588
- Lee U., 2001, ApJ, 557, 311
- Lee U., 2006, MNRAS, 365, 677
- Lee U., Saio H., 1989, MNRAS, 237, 875
- Lee U., Saio H., 1997, ApJ, 491, 839
- Osaki Y., 1986, PASP, 98, 30
- Pamyatnykh A. A., 1999, Acta Astron., 49, 119
- Penrod G. D., 1986, PASP, 98, 35
- Savonije G. J., 2005, A&A, 443, 557
- Townsend R. H. D., 2003a, MNRAS, 340, 1020
- Townsend R. H. D., 2003b, MNRAS, 343, 125
- Townsend R. H. D., 2005a, MNRAS, 360, 465
- Townsend R. H. D., 2005b, MNRAS, 364, 573

Walker G. A. H., Kuschnig R., Matthews J. M., et al., 2005,  
ApJ, 635, L77